Dalton Transactions

ROYAL SOCIETY OF CHEMISTRY

PAPER

Published on 03 July 2026

Cite this: *Dalton Trans.*, 2026, **55**, 10931

A molecular 'LEGO®' approach to high-spin triangular $\{Mn^{III}Ln_2\}$ clusters from $\{Mn^{III}\}$ and $\{Ln_2\}$ metalloligands

Konstantinos N. Pantelis,[a] Luís Cunha-Silva,[b,c] Mohamed R. Saber,†[d] Kim R. Dunbar,*[d] Dimitris I. Alexandropoulos*[a] and Theocharis C. Stamatatos*[a]

A stepwise "LEGO®-brick" strategy has been employed for the targeted assembly of rare low-nuclearity Mn^{III}/Ln^{III} clusters from preformed molecular building units. The mononuclear Mn^{III} metalloligand $(Pr_2NH_2)[Mn^{III}(sacb)_2]$ (**1**; $sacbH_2$ = *N*-salicylidene-2-amino-5-chlorobenzoic acid) was combined with newly isolated dinuclear lanthanide complexes $[Ln_2(sacb)(sacbH)_3L(MeOH)]$ [Ln^{III} = Dy (**2**), Gd (**3**); L^- = 2-amino-5-chlorobenzoate], affording the trinuclear heterometallic compounds $[Mn^{III}Ln_2(sacb)_3(sacbH)_2L]$ [Ln^{III} = Dy (**4**), Gd (**5**)]. Single-crystal X-ray diffraction studies revealed that **4** and **5** possess triangular $\{Mn^{III}Ln_2(\mu\text{-}O_2CR)_3\}^{6+}$ cores, representing the first structurally characterized triangular $\{Mn^{III}Ln_2\}$ complexes and rare examples of triangular $\{MLn_2\}$ (M = any 3d-metal ion) clusters. Magnetic studies have demonstrated that the Mn^{III}-free $\{Dy_2\}$ precursor **2** displays weak field-induced slow relaxation of magnetization, whereas incorporation of the Jahn–Teller active Mn^{III} ion leads to ferromagnetically coupled $\{Mn^{III}Ln_2\}$ species. In particular, the $\{Mn^{III}Gd_2\}$ analogue **5** exhibits a high-spin ground state of S = 9, with weak ferromagnetic $Mn^{III}\cdots Gd^{III}$ and $Gd^{III}\cdots Gd^{III}$ exchange interactions. Although no slow magnetic relaxation was observed for the trinuclear complexes, the results demonstrate that controlled integration of a Mn^{III} metalloligand can promote ferromagnetic exchange in preassembled $\{Ln_2\}$ units and provide a direct route to structurally defined high-spin 3d/4f triangles.

Received 11th June 2026,
Accepted 1st July 2026

DOI: 10.1039/d6dt01428c

rsc.li/dalton

1. Introduction

Since the emergence of single-molecule magnets (SMMs) as a distinct class of molecular magnetic materials,[1,2] Mn^{III}-containing clusters have attracted sustained interest in molecular magnetism because octahedral Jahn–Teller active Mn^{III} ions combine high-spin values, appreciable magnetic anisotropy, and a marked tendency to assemble into polymetallic architectures of diverse nuclearity and topology. These features have made Mn^{III} a particularly valuable metal ion in the development of molecule-based magnetic materials and the establishment of magnetostructural correlations in polynuclear systems.[3] At the same time, trivalent lanthanide (Ln) ions have become central to modern SMM chemistry owing to their large single-ion anisotropies, which originate from strong spin–orbit coupling and the crystal-field splitting of the 4f electronic states.[4–8] From this perspective, the combination of Mn^{III} and Ln^{III} ions within the same molecular framework is especially attractive, since it offers the opportunity to merge the structural versatility and exchange pathways of Mn^{III} centers with the strong anisotropy and distinctive magnetic behavior of lanthanide ions.[9,10]

Despite this promise, the chemistry and magnetism of heterometallic Mn/Ln clusters remain challenging. A variety of Mn/Ln SMMs have been reported, including $\{Mn^{III}_6Ln_2\}$,[11a] $\{Mn^{III}_4Mn^{IV}Ln_4\}$,[11b] $\{Mn^{III}_4Mn^{IV}_2Dy_6\}$,[11c] $\{Mn^{III}_9Mn^{II}_2Gd_2\}$,[11d] $\{Mn^{III}_{11}Mn^{II}Gd\}$,[11e] $\{Mn^{III}_{11}Ln_4\}$,[11f] $\{Mn^{III}_{12}Dy_6\}$,[11g] $\{Mn^{II}_6Mn^{III}_{12}Dy\}$[11h] and $\{Mn^{III}_{18}Mn^{IV}_3Dy\}$[11i] but the majority are high-nuclearity species whose magnetochemical interpretation is complicated by multiple, often inequivalent, exchange pathways, possible spin frustration, strong spin–orbit coupling effects, and the generally weak Mn–Ln and Ln–Ln magnetic interactions.[11] As a result, the extraction of meaningful magnetostructural correlations from high-nuclearity systems is not straightforward. In this context, low-nuclearity Mn^{III}/Ln^{III} complexes are particu-

[a]*Department of Chemistry, University of Patras, Patras 26504, Greece. E-mail: kostaspantelis95@gmail.com, dalexandrop4@gmail.com, thstama@upatras.gr*
[b]*LAQV/REQUIMTE & Department of Chemistry and Biochemistry, Faculty of Sciences, University of Porto, 4169-007 Porto, Portugal*
[c]*LNEG – National Laboratory of Energy and Geology IP, Campus of Lumiar, 1649-038 Lisboa, Portugal. E-mail: luis.csilva@lneg.pt*
[d]*Department of Chemistry, Texas A&M University, College Station, Texas 77843, USA. E-mail: dunbar@chem.tamu.edu*
† Present address: Chemistry Department, Faculty of Science, Fayoum University, Fayoum 63514, Egypt. E-mail: mrm01@fayoum.edu.eg

larly important, as they provide more tractable model systems for probing the nature, magnitude, and structural origin of magnetic exchange interactions between 3d and 4f metal centers. Among such targets, trinuclear triangular species are especially appealing because they combine structural simplicity with chemically and magnetically appealing topologies. Their well-defined metal arrangements make them attractive platforms for investigating exchange coupling, spin alignment, and the influence of bridging ligands on magnetic behavior. Although homometallic 3d and 4f triangles are well documented,[12] heterometallic 3d/4f triangular analogues remain comparatively rare.[13]

Access to low-nuclearity Mn^{III}-containing clusters is itself nontrivial. A longstanding synthetic difficulty in Mn^{III} coordination chemistry lies in the stabilization of the +3 oxidation state, which is crucial for preserving the characteristic Jahn–Teller distortion and magnetic properties of this ion.[14] Most Mn^{III} complexes are obtained through self-assembly processes in which suitable chelating and/or bridging ligands assist the mild oxidation of Mn^{II} to Mn^{III}, often under aerobic conditions, while simultaneously providing thermodynamic stabilization and structural integrity to the resulting products.[1b] Although highly successful, this approach can also lead to complex product mixtures or to compounds whose nuclearity and topology are difficult to predict. An attractive alternative is the "metal complexes as ligands" strategy, also referred to as the metalloligand approach, in which preformed low-nuclearity metal complexes bearing accessible donor atoms are used as secondary building units for the construction of more elaborate architectures.[15]

Within this context, Schiff-base ligands continue to play a prominent role in coordination chemistry because of their versatile binding modes, their ability to support multiple nuclearities, and their effectiveness in stabilizing transition metal and lanthanide ions in a wide variety of coordination environments. Our group has extensively explored the coordination chemistry of *N*-salicylidene-2-amino-5-chlorobenzoic acid ($sacbH_2$, Fig. 1), a ligand that, upon deprotonation, has proven highly effective in stabilizing oligonuclear $Mn^{II/III}$ and Dy^{III} species, as well as a broad family of polynuclear 3d, 3d/3d′, and 3d/4f complexes with interesting motifs.[16] The dianionic form of $sacb^{2-}$ provides a means of fostering the coordination of both hard and soft Lewis acids, *i.e.* 3d- and 4f-metal ions in moderate-to-high oxidation states, through the use of varying hardness donor atoms, such as the imino nitrogen atom, and the phenolate and carboxylate oxygen atoms.

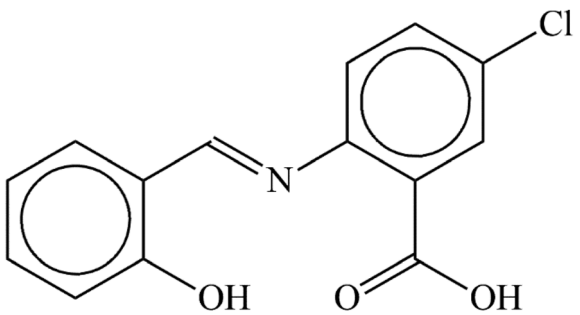

Fig. 1 Structural formula of the Schiff base ligand *N*-salicylidene-2-amino-5-chlorobenzoic acid ($sacbH_2$) employed in this work.

Particularly relevant to the present work is the previously reported mononuclear complex $(Pr_2NH_2)[Mn^{III}(sacb)_2]$ (**1**), which can function as an efficient Mn^{III} metalloligand through the dangling carboxylate O atoms of its $sacb^{2-}$ ligands.[16a] This feature makes **1** a promising preorganized building block for the targeted assembly of heterometallic Mn^{III}/Ln^{III} species.

Herein, we build on this concept by combining complex **1** with the new dinuclear lanthanide precursors, $[Ln_2(sacb)(sacbH)_3L(MeOH)]$ (Ln^{III} = Dy (**2**), Gd (**3**); L^- = 2-amino-5-chlorobenzoate), in order to construct low-nuclearity heterometallic 3d/4f clusters through a "LEGO®-brick" synthetic strategy. This approach has afforded the ferromagnetically-coupled, triangular complexes $[Mn^{III}Ln_2(sacb)_3(sacbH)_2L]$ (Ln^{III} = Dy (**4**), Gd (**5**)), thus providing new examples of structurally defined Mn^{III}/Ln^{III} high-spin assemblies derived from preformed mono- and dinuclear building blocks.

2. Experimental section

a. Materials, physical and spectroscopic measurements

All manipulations were performed under aerobic conditions using materials (reagent grade) and solvents as received unless otherwise noted. The Schiff base ligand $sacbH_2$ was prepared, purified, and characterized as described elsewhere.[16e] The coordinated ligand L^- (anion of 2-amino-5-chlorobenzoic acid) in complexes **2–5** (*vide infra*) is the hydrolysis product of the employed ligand $sacbH_2$. Elemental analyses (C, H, and N) were performed by the University of Patras microanalytical service. Infrared (IR) spectra (4000–400 cm^{-1}) were recorded in the solid state using a PerkinElmer 16 PC spectrometer with samples prepared as KBr pellets. Powder-XRD diffraction patterns for **2** and **3** were recorded on a Rigaku Miniflex 6G X-ray diffractometer (Cu Kα radiation, λ = 1.5418 Å). Variable-temperature direct and alternating current (dc and ac, respectively) magnetic susceptibility studies were conducted on a Quantum Design MPMS XL-7 SQUID magnetometer equipped with a 7 T magnet in the temperature range of 2–300 K. Diamagnetic corrections were applied to the observed paramagnetic susceptibility using Pascal's constants.[17]

b. Synthesis of $(Pr_2NH_2)[Mn^{III}(sacb)_2]$ (1)

The preparation and crystallization of **1** was carried out as described elsewhere.[16a] Briefly, the reaction of $Mn(O_2CMe)_2{\cdot}4H_2O$ (0.05 g, 0.20 mmol), $sacbH_2$ (0.11 g, 0.40 mmol) and Pr_2NH (82 μL, 0.60 mmol) in solvent MeOH (15 mL), has led to a brown-red microcrystalline solid of **1** in excellent yields (~90%).

c. Synthesis of $[Dy_2(sacb)(sacbH)_3L(MeOH)]$ (2)

To a stirred yellowish solution of $sacbH_2$ (0.05 g, 0.20 mmol) in a solvent mixture comprising $MeOH/CH_2Cl_2$ (12 mL, 2 : 1

v/v) was added solid $Dy(O_2CMe)_3{\cdot}4H_2O$ (0.04 g, 0.10 mmol). The resulting orange solution was stirred for 40 min, during which time an orange microcrystalline solid was formed. This material was collected by filtration, washed with cold MeOH (2 × 3 mL), and dried under vacuum. Light orange single crystals suitable for X-ray diffraction studies were grown after 15 days from a slow evaporation process of the resulting filtrate at room temperature and were analyzed as **2**. The IR spectrum of the orange microcrystalline material was identical to that of the air dried, single crystals of **2**. The yield of the orange microcrystalline solid was 81% (based on the organic chelate available). Anal. calc. for $C_{64}Cl_5H_{44}N_5O_{15}Dy_2$ (found values in parentheses): C 47.30% (47.33%), H 2.73% (2.85%) and N 4.31% (4.37%). Selected IR data (KBr, cm^{-1}) = 3460 (m), 1615 (s), 1526 (m), 1462 (w), 1417 (w), 1377 (m), 1231 (m), 1180 (w), 1146 (m), 1110 (w), 1019 (w) 890 (w), 854 (w), 819 (w), 761 (w), 721 (w), 651 (w), 572 (w), 529 (w), 492 (w), 470 (w), 451 (m).

d. Synthesis of $[Gd_2(sacb)(sacbH)_3L(MeOH)]$ (3)

Orange microcrystalline solid of **3** was prepared in the exact same manner as complex **2** but using $Gd(O_2CMe)_3{\cdot}4H_2O$ (0.04 g, 0.10 mmol) as the lanthanide source. The solid was collected by filtration, washed with cold MeOH (2 × 3 mL) and dried in air (yield as high as 75%). Unfortunately, we were not able to obtain single crystals of **3**, but we have further confirmed the identity of this compound by: (i) comparing p-XRD (Fig. S1) and IR spectra (Fig. S2) with the authentic, single-crystalline sample of **2**, and (ii) conducting elemental analyses. Anal. calc. for **3** (found values in parentheses): C 47.60% (47.65%), H 2.75% (2.86%) and N 4.34% (4.32%).

e. Synthesis of $[Mn^{III}Dy_2(sacb)_3(sacbH)_2L]$ (4)

To a stirred, brown-red slurry of the $(Pr_2NH_2)[Mn^{III}(sacb)_2]$ (**1**) precursor (0.01 g, 0.02 mmol) in solvent MeCN (15 mL) was added solid complex $[Dy_2(sacb)(sacbH)_3L(MeOH)]$ (**2**) (0.03 g, 0.02 mmol). The resulting olive-brown slurry was refluxed for 1 h, during which time all solids dissolved, and the color of the solution remained olive-brown. The solution was then filtered, and the filtrate was allowed to evaporate slowly at room temperature. After 9 days, X-ray quality well-formed brown crystals of **4** appeared, and these were collected by filtration and washed with cold MeCN (2 × 3 mL) and Et_2O (2 × 5 mL). The yield was 42% (based on the organic chelate available). Upon dryness (under vacuum) the crystalline solid was analyzed as **4**. Anal. calc. for $C_{77}Cl_6H_{47}N_6O_{17}Dy_2Mn$ (found values in parentheses): C 48.15% (48.11%), H 2.47% (2.43%) and N 4.38% (4.42%). Selected IR data (KBr, cm^{-1}) = 3443 (w), 1605 (s), 1542 (w), 1470 (w), 1446 (w), 1417 (w), 1370 (w), 1298 (w), 1229 (m), 1186 (w), 1149 (m) 1116 (w), 1020 (w), 901 (w), 856 (w), 824 (w), 805 (w), 762 (w), 738 (w), 721 (w), 642 (w), 594 (w), 568 (w), 533 (w), 476 (w), 441 (w).

f. Synthesis of $[Mn^{III}Gd_2(sacb)_3(sacbH)_2L]$ (5)

X-ray-quality crystals of complex **5** were prepared following the same procedure used for complex **4**, but employing $[Gd_2(sacb)(sacbH)_3L(MeOH)]$ (0.03 g, 0.02 mmol) complex **3** as the lanthanide precursor. The crystals were collected by filtration, washed with cold MeCN (2 × 3 mL) and Et_2O (2 × 5 mL), and dried under vacuum to afford an overall 36% yield (based on the total available organic chelate). The identity of **5** was further confirmed by (i) comparison of its IR spectrum with that of the single-crystalline sample of **4** (Fig. S3) and (ii) elemental analysis. Anal. calc. for $C_{77}Cl_6H_{47}N_6O_{17}Gd_2Mn$ (found values in parentheses): C 48.33% (48.41%), H 2.27% (2.48%) and N 4.28% (4.40%).

g. Single-crystal X-ray crystallography

Light orange single crystals of complex **2** (0.03 × 0.02 × 0.02 mm) and brown single crystals of complexes **4** (0.16 × 0.06 × 0.02 mm) and **5** (0.19 × 0.09 × 0.07 mm), were mounted onto a cryoloop using adequate inert oil,[18] and immediately cooled at 173 K (for **2**) and 150 K (for **4** and **5**). X-ray diffraction data for **2** were collected on a Rigaku Oxford Diffraction XtaLAB Synergy diffractometer equipped with a HyPix-6000HE area detector and using Cu Kα monochromated radiation (λ = 1.54184 Å) from a PhotonJet microfocus source. For complexes **4** and **5**, X-ray diffraction data were collected on a Bruker X8 Kappa APEX II Charge-Coupled Device (CCD) area-detector diffractometer controlled by the APEX2[19] software package (Mo Kα graphite-monochromated radiation, λ = 0.71073 Å) and equipped with an Oxford Cryosystems Series 700 cryostream monitored remotely with the software interface Cryopad.[20] Data processing was performed with SAINT,[21] and absorption corrections were applied using the multiscan method in SADABS.[22] All structures were solved using the charge-flipping algorithm in SUPERFLIP,[23] and refined using full-matrix least-squares techniques on F^2 with SHELXL[24a] through the OLEX2[24b] interface. Non-hydrogen atoms were successfully refined anisotropically. Hydrogen atoms bonded to carbon and hydroxide groups were placed at idealized positions using appropriate HFIX instructions in SHELXL or located from different Fourier maps and refined isotropically. Some additional electron density was found in the data of complexes **4** and **5**, probably due to disordered solvent molecules. Efforts to accurately locate, model and refine these residues were ineffective, and the investigation for the total potential solvent area using the software package PLATON[25a,b] confirmed the existence of cavities with potential solvent accessible void volume. Thus, the original data sets were treated with the program routine SQUEEZE.[25c] Various figures of all structures were generated, using Diamond 3[26] and Mercury[27] software packages. The unit cell parameters, structure solution, and refinement details of compounds **2**, **4** and **5** are summarized in Tables S1 and S2. Further crystallographic details are available in the corresponding CIF files provided in the SI.

3. Results and discussion

a. Synthetic comments and IR spectra

The previously reported metalloligand $(Pr_2NH_2)[Mn^{III}(sacb)_2]$ (**1**) was employed as the Mn^{III}-containing building block for

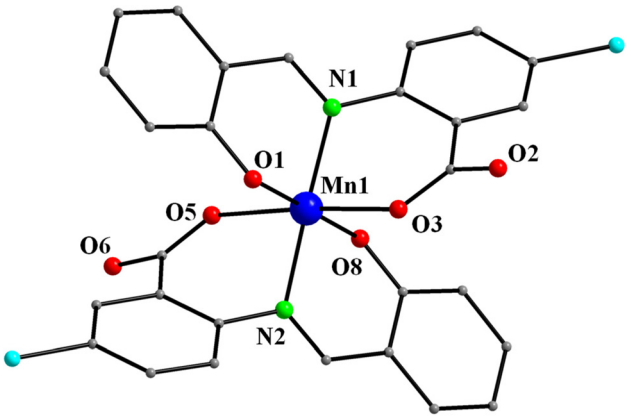

Fig. 2 Partially labeled representation of the previously reported structure of the anionic complex $[Mn^{III}(sacb)_2]^-$ (**1**). All H atoms are omitted for clarity. Color scheme: Mn^{III}, blue; O, red; N, green; C, gray; Cl, cyan.

the assembly of the heterometallic Mn^{III}/Ln^{III} products. Its molecular structure is shown in Fig. 2.[16a] Complex **1** contains a preformed $\{Mn^{III}(sacb)_2\}^-$ unit with free carboxylate O atoms, rendering it a suitable species for further binding to oxophilic Ln^{III} ions. Thus, its use allows direct incorporation of a structurally defined Mn^{III} fragment into the final heterometallic complexes, while avoiding uncontrolled Mn^{II}/Mn^{III} redox processes during cluster assembly.

To identify an appropriate lanthanide precursor for combination with the Mn^{III} metalloligand, we were guided by our previous work on $sacbH_2$-based lanthanide chemistry, particularly the dinuclear SMM $[Dy_2(NO_3)_4(sacbH)_2(H_2O)_2(MeCN)_2]$.[16b] Although chemically related to that earlier $\{Dy_2\}$ compound, the present system differs in both the lanthanide source and the reaction medium, leading to new dinuclear complexes with distinct ligand compositions and coordination environments. We therefore examined the reactivity of the organic chelate $sacbH_2$ with different Ln^{III} sources under a variety of conditions, including changes in the metal salt, solvent, reactant ratio, base, reaction time, temperature, concentration and crystallization method. From the reaction of $Ln(O_2CMe)_3{\cdot}4H_2O$ with $sacbH_2$ in a 1 : 2 molar ratio in a $MeOH/CH_2Cl_2$ solvent mixture, we isolated crystals of the dinuclear complexes $[Ln_2(sacb)(sacbH)_3L(MeOH)]$ (Ln^{III} = Dy (**2**), Gd (**3**); L^- = 2-amino-5-chlorobenzoate) in yields as high as 81% and 75%, respectively. The coordinated 2-amino-5-chlorobenzoate group (L^-) originates from partial metal-ion-assisted hydrolysis of $sacbH_2$, a process previously observed in related systems.[16f] Although acetate ions are not incorporated into the final products, they likely act as proton acceptors, assisting the complete or partial deprotonation of the organic chelate. Complexes **2** and **3** were obtained as crystalline, air- and moisture-stable solids under ambient conditions. Their crystallinity was found to depend strongly on both the solvent mixture and the molar ratio of the starting materials. Altering these parameters, or using external organic bases such as NMe_3, NEt_3, NPr_3, $NHMe_2$, $NHEt_2$, $NHPr_2$, led only to microcrystalline materials, which were identified as **2** and **3** by IR spectroscopy and elemental analysis. In contrast, when the reactions were carried out solely in MeOH, only oily or amorphous materials were obtained, preventing further characterization.

Negative (−) and positive (+) ion ES-MS studies were then performed in MeCN to evaluate whether the potential building blocks **1** and **2** preserve their main molecular fragments in solution. The spectra showed intense signals at m/z = 600.72 and 1312.79, assigned to the singly charged $\{Mn(sacb)_2\}^-$ and $\{Dy_2(sacb)(sacbH)_2L\}^+$ fragments of **1** and **2**, respectively (Fig. S4). These observations support the idea that the Mn^{III} and Ln^{III}-containing units of **1** and **2** retain sufficient structural integrity in MeCN to behave as complementary "LEGO®-bricks" during the subsequent assembly process.

On this basis, precursor **1** was reacted with either **2** or the isomorphous **3** in equimolar ratios in MeCN under refluxing (to enhance their solubilities) conditions. These structure-directed reactions successfully afforded brown crystalline trinuclear compounds with the general formula $[Mn^{III}Ln_2(sacb)_3(sacbH)_2L]$ (Ln^{III} = Dy (**4**), Gd (**5**); L^- = 2-amino-5-chlorobenzoate) in 42% and 36% yields, respectively. The formation of **4** and **5** highlights the synthetic value of the "metal complexes as ligands" strategy. The preformed $\{Mn^{III}(sacb)_2\}^-$ and $\{Ln_2(sacb)(sacbH)_2L\}^+$ fragments appear to act as complementary building blocks, with the available carboxylate O atoms of the Mn^{III} metalloligand bridging to the lanthanide centers of the dinuclear precursor. This stepwise approach proved essential, since extensive attempts to prepare the same crystalline heterometallic products through direct one-pot reactions between $MnX_2{\cdot}xH_2O$, $LnX_3{\cdot}xH_2O$ ($X^- = NO_3^-$, Cl^-, $MeCO_2^-$, ClO_4^-, *etc.*) and $sacbH_2$ under various solvents, bases and crystallization conditions were unsuccessful. These reactions typically afforded either the homometallic compounds **1–3** or poorly defined microcrystalline/amorphous materials. Moreover, MeCN was found to be crucial for the formation and crystallization of **4** and **5**; reactions in MeOH, EtOH or CH_2Cl_2 did not yield the desired heterometallic products.

The IR spectra of complexes **2** and **4** are discussed as representative examples, since the isomorphous analogues **3** and **5** display very similar spectra. In complex **2**, the weak band at 3460 cm^{-1} is consistent with the presence of the coordinated MeOH molecule. Both complexes show several bands in the ~1542–1229 cm^{-1} region, mainly associated with aromatic-ring vibrations of the $sacb^{2-}$, $sacbH^-$ and L^- ligands. These overlap with carboxylate stretching bands, resulting in mixed vibrations that hinder precise assignments. Notably, strong bands at 1615 cm^{-1} (for **2**) and 1605 cm^{-1} (for **4**) are attributed to the ν(C=N) stretching of the coordinated $sacb^{2-}$ and $sacbH^-$ ligands.[28]

b. Description of structures

Compounds $[Dy_2(sacb)(sacbH)_3L(MeOH)]$ (**2**) and $[Mn^{III}Dy_2(sacb)_3(sacbH)_2L]$ (**4**) crystallize in the triclinic $P\bar{1}$ space group, whereas $[Mn^{III}Gd_2(sacb)_3(sacbH)_2L]$ (**5**) crystallizes in the monoclinic $C2/c$ space group. Given the close struc-

tural resemblance of **4** and **5**, the former complex is discussed in detail as a representative example, while further structural discussions highlight their magnetochemical properties. Selected interatomic distances and bond angles for the Dy-containing complexes **2** and **4** are provided in Tables S3 and S4, respectively. The oxidation states of Mn centers in **4** and **5** were confirmed by charge balance and bond valence sum (BVS) analyses (Table S5), establishing Mn ion in the +III oxidation state.[29]

The molecular structure of $[Dy_2(sacb)(sacbH)_3L(MeOH)]$ (**2**) is depicted in Fig. 3. The two Dy^{III} ions are doubly bridged by the deprotonated carboxylate-O atoms (O2, O10, O7, O9) from two $\eta^1{:}\eta^1{:}\eta^1{:}\mu$ $sacbH^-$ ligands and one μ-O_2CR group (O1) derived from a $\eta^1{:}\eta^1{:}\eta^2{:}\eta^1{:}\mu$ $sacb^{2-}$ ligand, resulting in a $\{Dy_2(\mu\text{-}O_2CR)_3\}^{3+}$ subunit with a Dy1···Dy2 separation of 4.575 (4) Å. The single μ-O bridge (O1) results in a Dy1–O1–Dy2 angle of 135.5(1)°, and the central core is further supported by the double $\eta^1{:}\eta^1{:}\mu$ carboxylate bridges of two $sacbH^-$ chelates (Fig. 4a). The Dy1 center completes eight-coordination through a chelating $\eta^1{:}\eta^1$ L^- ligand (O11, O14), one imino-N atom from a $sacb^{2-}$ group, and two terminal phenoxo-O atoms from $sacbH^-$ (O5) and $sacb^{2-}$ (O6) ligands. Similarly, the Dy2 center is eight-coordinated with its coordination sphere being completed by a terminal $\eta^1{:}\eta^1$ $sacbH^-$ ligand (O4, O12), one terminal carboxylate-O atom (O3) from a $sacb^{2-}$ ligand, one phenoxo-O atom (O13) from a $sacbH^-$ ligand, and a terminally bound MeOH (O15) solvate molecule. Proton transfer from the phenol groups of the three $sacbH^-$ ligands to the imino-N atoms renders the latter positively charged and uncoordinated. The coordination modes of all ligands in **2** are summarized in Fig. 4b.

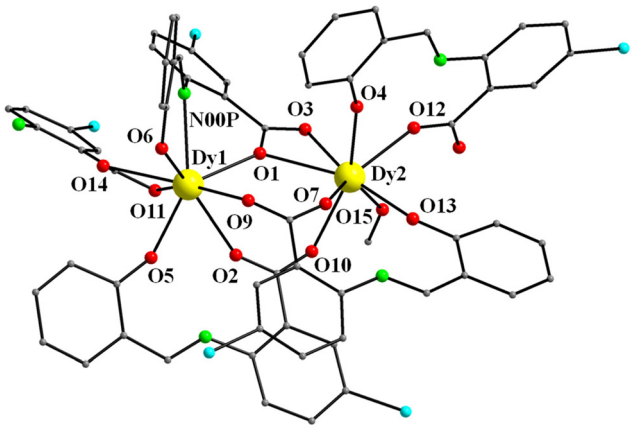

Fig. 3 Partially labeled representation of the molecular structure of $[Dy_2(sacb)(sacbH)_3L(MeOH)]$ (**2**) complex. All H atoms are omitted for clarity. Color scheme: Dy^{III}, yellow; O, red; N, green; C, gray; Cl, cyan.

The coordination environments of Dy1 and Dy2 ions were further analysed by Continuous Shape Measure (CShM) calculations using the SHAPE program (Table S6), which quantify the deviation of a given metal coordination polyhedron from ideal reference geometries.[30,31] For Dy1, the lowest CShM value corresponds to a biaugmented trigonal prism (CShM = 1.77; virtual C_{2v} point-group symmetry), whereas the coordination environment of Dy2 is best described as a triangular dodecahedron (CShM = 1.67; virtual D_{2d} point-group symmetry), as illustrated in Fig. S5.

The crystal structure of **2** is stabilized by seven strong intramolecular H bonds (Fig. S6). One involves the terminal L^- ligand, characterized by an $NH_L\cdots O_L$ distance of 2.655(5) Å. The remaining H bonds are formed between carboxylate/phenoxo-O atoms and the N–H groups of $sacbH^-$ ligands, with separations ranging from 2.569(5) to 2.645(5) Å. From a supra-

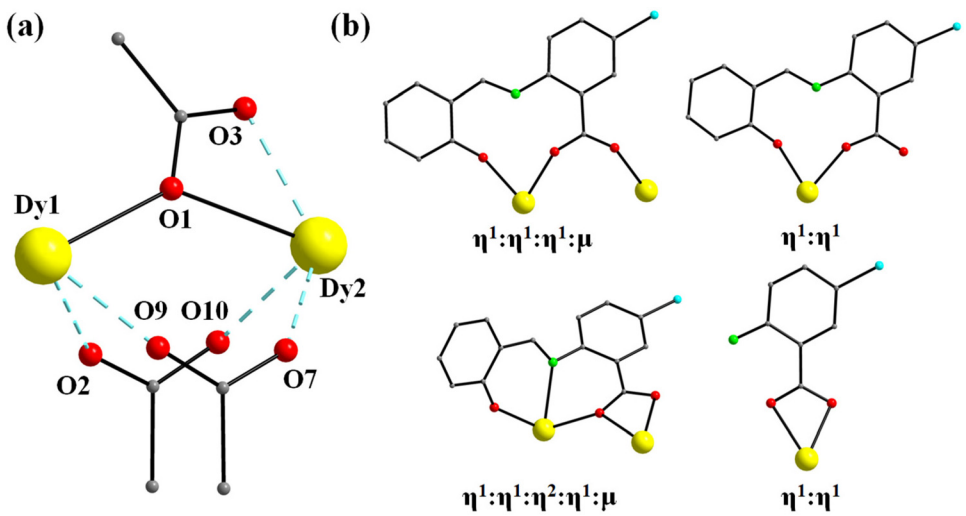

Fig. 4 (a) The labeled $\{Dy_2(\mu\text{-}O_2CR)_3\}^{3+}$ core of **2**, highlighting with cyan dashed lines the additional Dy–O bonds provided by one bidentate bridging/chelating carboxylate group (O3) from the $sacb^{2-}$ and two bidentate bridging carboxylate groups (O2, O7, O9, O10) from the $sacbH^-$ ligands. (b) The crystallographically established coordination modes of $sacb^{2-}$, $sacbH^-$ and L^- ligands. All H atoms are omitted for clarity. Color scheme: Dy^{III}, yellow; O, red; N, green; C, gray; Cl, cyan.

molecular standpoint, intermolecular interactions between the dinuclear complexes are negligible, indicating that the molecules remain well isolated in the lattice. The $\{Dy_2\}$ units adopt a helical conformation along the crystallographic *c*-axis, with the shortest Dy···Dy separation between these units being 9.660(1) Å (Fig. S7).

The molecular fragments $\{Mn(sacb)_2\}^-$ and $\{Dy_2(sacb)(sacbH)_2L\}^+$, identified by ES-MS studies, of **1** and **2**, respectively, are shown in Fig. 5 together with the molecular structure of the resulting $[Mn^{III}Dy_2(sacb)_3(sacbH)_2L]$ (**4**) complex, to illustrate the structural relationship between the precursor fragments and the final trinuclear heterometallic cluster. In **4**, the three metal ions are connected through five carboxylate bridges: two bidentate bridging carboxylate groups, defined by O8/O9 and O11/O12, from two $\eta^1{:}\eta^1{:}\eta^1{:}\mu$ $sacbH^-$ ligands, and three monoatomic μ-O_2CR bridges, O1, O2 and O3, derived from three $\eta^1{:}\eta^1{:}\eta^2{:}\eta^1{:}\mu$ $sacb^{2-}$ ligands. This connectivity generates a $\{Mn^{III}Dy_2(\mu\text{-}O_2CR)_5\}^{4+}$ subunit, with metal···metal separations of Dy1···Dy2 = 4.416(4) Å, Mn1···Dy1 = 4.519(4) Å and Mn1···Dy2 = 4.267(4) Å. If the two bidentate carboxylate bridges are excluded, the metal core may be described as a triangular scalene $\{Mn^{III}Dy_2(\mu\text{-}O_2CR)_3\}^{6+}$ unit, with Dy1–O1–Dy2, Mn1–O3–Dy1 and Mn1–O2–Dy2 angles of 131.7(2)°, 144.9(3)° and 138.4(2)°, respectively (Fig. 6a). To the best of our knowledge, this type of triangular $\{Mn^{III}Dy_2(\mu\text{-}O_2CR)_3\}^{6+}$ core has not previously been reported in 3d/4f-metal cluster chemistry.

A clear structural relationship exists between the $\{Dy_2(\mu\text{-}O_2CR)_3\}^{3+}$ subunit of **2** and the $\{Mn^{III}Dy_2(\mu\text{-}O_2CR)_5\}^{4+}$ subunit within **4**. The latter can be viewed as resulting from the incorporation of an additional $\{Mn^{III}(sacb)_2\}^-$ fragment into the dinuclear dysprosium framework. This $\{Mn^{III}(sacb)_2\}^-$ fragment originates from complex **1**, in which the carboxylate O atoms of the two $sacb^{2-}$ ligands provide additional bridging sites toward the Dy^{III} centers of the $\{Dy_2(sacb)(sacbH)_2L\}^+$ unit of **2**. Therefore, coordination of the Mn^{III} metalloligand to available sites on the $\{Dy_2\}$ precursor leads to the assembly of the trinuclear $\{Mn^{III}Dy_2\}$ core, as shown in Fig. 5.

The three $sacb^{2-}$ ligands in **4** display a dual coordination role. Each ligand chelates one metal ion through phenoxo-O, imino-N and carboxylate-O donor atoms, while its carboxylate group also bridges to an additional Dy^{III} center. The two $sacbH^-$ ligands bind only to Dy^{III} ions through O-donor atoms and, as in complex **2**, undergo intra-ligand proton transfer from the phenolic O atom to the imino-N atom; the resulting protonated imino-N atoms are therefore non-coordinating. The Dy1 coordination environment is further supported by two O-donor atoms from the terminal $\eta^1{:}\eta^1$ L^- ligand, where L^- is the anion of 2-amino-5-chlorobenzoic acid. The coordination modes of the $sacb^{2-}$, $sacbH^-$ and L^- ligands in **4** are summarized in Fig. 6b.

In complexes **4** and **5**, the Mn^{III} centers are six-coordinate, adopting distorted octahedral geometries. Their environments are best described as Jahn–Teller distorted octahedral, with two elongated axial bonds involving one carboxylate-O atom (Mn–O = 2.121(5) Å for **4**, 2.126(6) Å for **5**) and one imino-N atom (Mn–N = 2.152(6) Å for **4**, 2.154(7) Å for **5**) from $sacb^{2-}$ ligands. The equatorial planes are occupied by two phenoxo-O, one carboxylate-O, and one imino-N atom, also from $sacb^{2-}$ ligands. The Dy1 ion in **4** and the Gd1 ion in **5** are each nine-coordinate, surrounded exclusively by O-donor atoms, giving

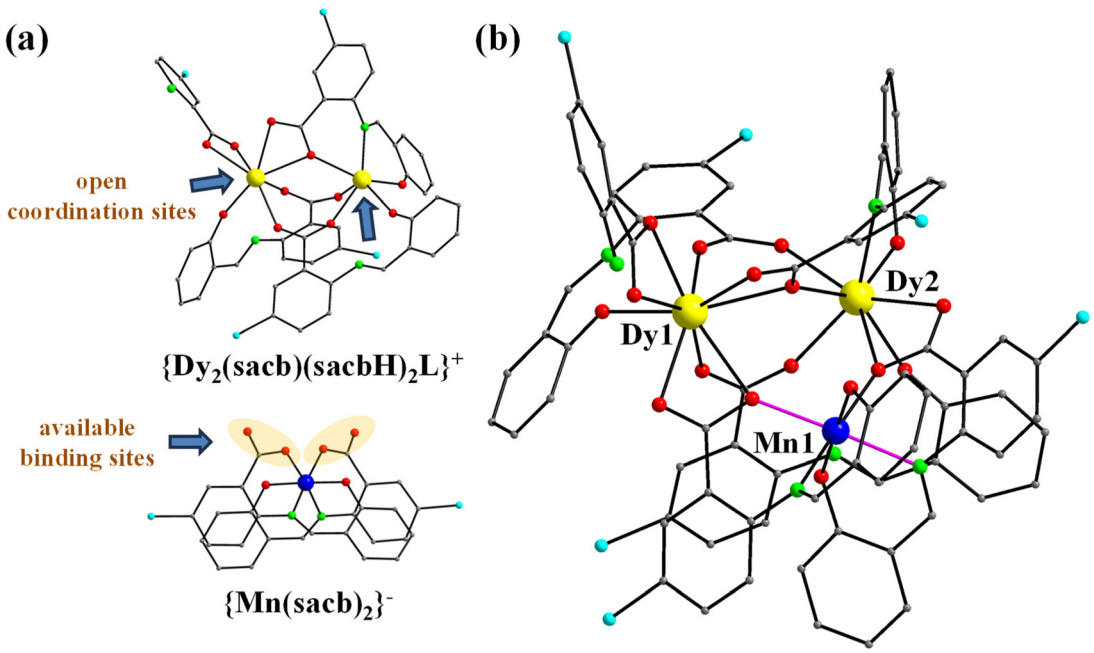

Fig. 5 (a) The molecular structures of the $\{Mn(sacb)_2\}^-$ and $\{Dy_2(sacb)(sacbH)_2L\}^+$ fragments employed as "LEGO®-bricks". (b) Partially labeled representation of the molecular structure of complex $[Mn^{III}Dy_2(sacb)_3(sacbH)_2L]$ (**4**). The Mn^{III} Jahn–Teller axis is highlighted with purple coloration. All H atoms are omitted for clarity. Color scheme: Dy^{III}, yellow; Mn^{III}, blue; O, red; N, green; C, gray; Cl, cyan.

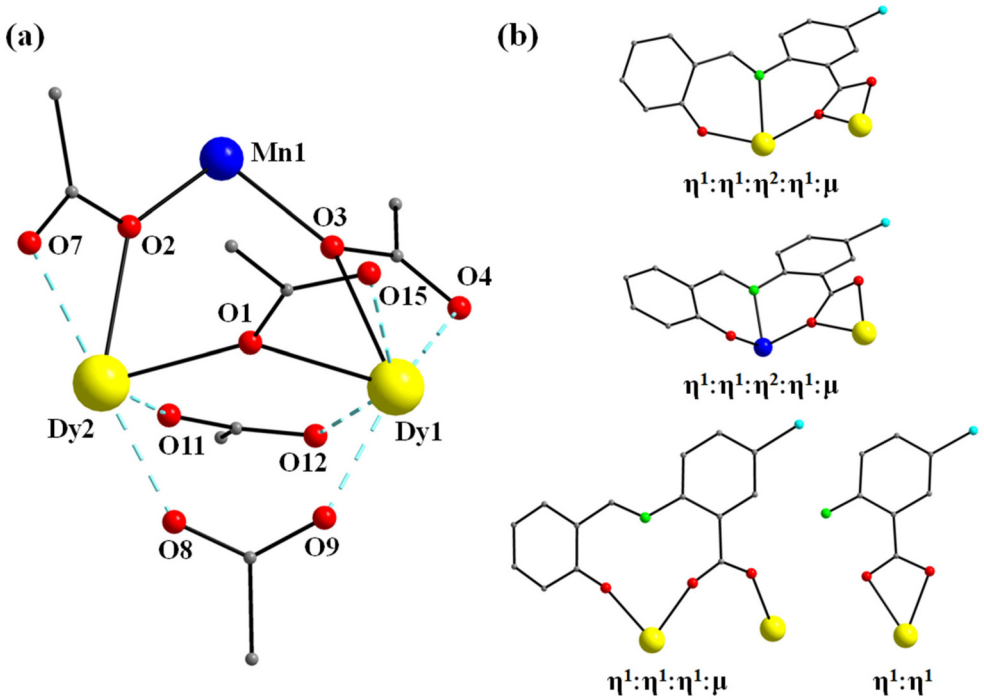

Fig. 6 (a) The labeled $\{Mn^{III}Dy_2(\mu\text{-}O_2CR)_3\}^{6+}$ core of **4**, highlighting with cyan dashed lines the additional Dy–O bonds provided by three tridentate bridging/chelating carboxylate groups (O4, O7, O15) from the $sacb^{2-}$ ligands and two bidentate bridging carboxylate groups (O8, O9, O11, O12) from the $sacbH^{-}$ ligands. (b) The crystallographically established coordination modes of $sacb^{2-}$, $sacbH^{-}$ and L^{-} ligands. All H atoms are omitted for clarity. Color scheme: Dy^{III}, yellow; Mn^{III}, blue; O, red; N, green; C, gray; Cl, cyan.

rise to muffin-type geometries (CShM = 2.06 for Dy1; 2.03 for Gd1) with virtual C_s point group symmetries. In contrast, the Dy2 ion in **4** and the Gd2 ion in **5** are eight-coordinate, bonded to seven O- and one N-donor atoms. Their geometries correspond to distorted square antiprisms (CShM = 1.43 for Dy2; 1.55 for Gd2), with virtual D_{4d} point group symmetries. All CShM values were determined, as for complex **2**, using the SHAPE program.[30] The representative coordination polyhedra of Dy1 and Dy2 atoms in complex **4** are shown in Fig. S8.

The crystal structures of complexes **4** and **5** are stabilized through four strong intramolecular H bonds. As illustrated in Fig. S9 for complex **4** (taken as a representative case), these interactions occur between the carboxylate/phenoxo-O atoms and the N–H groups of $sacbH^{-}$ ligands, with N–H···O distances spanning the range 2.607(9)–2.680(8) Å. Notably, **4** and **5** crystallize in different space groups (triclinic $P\bar{1}$ for **4** and monoclinic $C2/c$ for **5**) resulting in distinct supramolecular arrangements. Along the crystallographic *a*-axis, the $\{MnDy_2\}$ units in **4** form supramolecular pores (Fig. S10), whereas the $\{MnGd_2\}$ units in **5** adopt helical conformations (Fig. S11). The relatively large Mn···Mn (12.027(1) Å for **4**; 8.499(2) Å for **5**), Mn···Dy (9.407(1) Å for **4**; 9.874(2) Å for **5**) and Dy···Dy (8.291(1) Å for **4**; 8.253(2) Å for **5**) separations demonstrate that intermolecular interactions among the trinuclear complexes are almost negligible and the molecules are well isolated from one another.

Given the limited number of trinuclear $\{MnLn_2\}$ clusters reported to date, these species are summarized in Table 1 to enable comparison of their formulae, metal-core topologies and magnetic properties, particularly the nature of the dominant magnetic exchange interactions. The reported examples are predomi-

Table 1 To date characterized $\{MnLn_2\}$ complexes with diagnostic structural and magnetic information

Complex[a]	Metal topology	Magnetic features	Ref.
$[Mn^{II}Ln_2(sald)_8]$[b], Ln^{III} = Gd, Tb, Dy, Ho, Er	Linear	F/AF (Dy, Ho) AF (Gd, Tb, Er)	32*a*
$[Mn^{II}Ln_2(QCl)_8]$[c], Ln^{III} = Tb, Dy, Er	Linear	AF	32*b*
$[Mn^{III}Ln_2(O_2CPh)_2(TEOAH_2)_4](NO_3)_3$,[d] Ln^{III} = Gd, Tb	Linear	AF	32*c*
$[Mn^{IV}Gd_2O(O_2CPh)_3(O_2CMe)(dapdo)(dapdoH)_2]$[e]	Triangular	F	32*d*
$[Mn^{III}Ln_2(sacb)_3(sacbH)_2L]$, Ln^{III} = Gd, Dy	Triangular	F	t.w.

[a] Lattice solvate molecules have been omitted. [b] Ligand abbreviations: saldH = salicylaldehyde. [c] QClH = 5-chloro-8-quinolinolic acid. [d] $TEOAH_3$ = triethanolamine. [e] $dapdoH_2$ = 2,6-diacetylpyridine dioxime. AF = antiferromagnetic; F = ferromagnetic. t.w. = this work.

nantly linear and generally exhibit antiferromagnetic exchange interactions,[32a–c] with the notable exception of a triangular $\{Mn^{IV}Gd_2(\mu_3\text{-}O)\}^{8+}$ cluster, for which dominant ferromagnetic interactions and an S = 13/2 ground state have been reported.[32d] In this context, complexes **4** and **5** are particularly noteworthy, as they appear to represent the first triangular $\{Mn^{III}Ln_2\}$ compounds, where Ln^{III} = Dy or Gd. The only previously reported trinuclear $\{Mn^{III}Ln_2\}$ system contains Mn in the +III oxidation state but it adopts a linear rather than triangular topology.[32c] It should also be noted that most magnetically studied triangular 3d/4f systems belong to the $\{M_2Ln\}$ family, where M is a 3d-metal ion.[13c–i] By contrast, triangular $\{MLn_2\}$ clusters remain rare. Complexes **4** and **5** therefore constitute only the fourth reported examples of triangular $\{MLn_2\}$ compounds, following the aforementioned $\{Mn^{IV}Gd_2\}$ cluster,[32d] an antiferromagnetically coupled $\{Ni^{II}Ln_2\}$ family with Ln^{III} = Gd, Tb, Dy and Ho,[13a] and a $\{Cr^{III}Dy_2\}$ complex displaying weak SMM dynamics.[13b]

c. Magnetic studies

Compound **2** features an uncommon $\{Dy_2(\mu\text{-}O_2CR)_3\}^{3+}$ carboxylate-bridged subunit, comprising two bidentate and one monoatomic carboxylate bridges. The closest magnetically investigated analogues are $\{Dy_2(\mu\text{-}OR)_2(\mu\text{-}O_2CR)_2\}^{2+}$ systems, which contain two bidentate carboxylate and two monoatomic alkoxido bridges and typically display predominant antiferromagnetic exchange interactions, often accompanied by weak SMM behavior.[33] The magnetic properties of **2** were therefore examined by direct-current (dc) magnetic susceptibility measurements in the 2–300 K temperature range under an applied field of 0.1 T (Fig. 7). At 300 K, the $\chi_M T$ value of 27.77 $cm^3\ mol^{-1}$ K is in good agreement with the theoretical value of 28.34 $cm^3\ mol^{-1}$ K for two noninteracting Dy^{III} ions ($^6H_{15/2}$, S = 5/2, L = 5, g = 4/3). Upon cooling, the $\chi_M T$ product remains essentially constant till ~90 K, below which it decreases gradually to 21.66 $cm^3\ mol^{-1}$ K at 2 K. This decrease is primarily attributed to the depopulation of the crystal-field (CF) M_J states with a possible contribution from intramolecular antiferromagnetic exchange interactions between the Dy^{III} centers. Field-dependent magnetization measurements were performed at 1.9, 3 and 5 K. The M *vs.* H plots show a rapid increase at low fields, followed by a more gradual increase at higher fields, without reaching saturation up to 7 T (Fig. 7, inset). This behavior is characteristic of systems with unquenched magnetic anisotropy and/or low-lying excited states. Moreover, the magnetization value at 7 T and 1.9 K is ~14.3$N\mu_B$, appreciably lower than the theoretical value for two Dy^{III} ions (J = 15/2, g = 4/3, $M_S/N\mu_B = ngJ$ = 20.0$N\mu_B$), further reflecting the presence of crystal field induced anisotropy in **2**.

Alternating-current (ac) magnetic susceptibility measurements were performed on **2** in the absence of an applied dc field, using a 3.0 G ac field in the 2–20 K temperature range. Complex **2** exhibits frequency-dependent out-of-phase susceptibility tails of peaks below ~6 K in the χ''_M *vs.* T plot (Fig. S12), without the observation of well-defined maxima, suggesting fast relaxation of the magnetization, most likely dominated by quantum tunnelling of the magnetization (QTM). To partially suppress this relaxation pathway, ac susceptibility measurements were subsequently carried out in the presence of external dc fields. A qualitative analysis of the field dependence of χ''_M at 1000 Hz and 1.9 K (Fig. S13) indicated that there is no well-defined maximum, other than a peak located at 1300 Oe, to utilize for the suppression of the QTM process. Under the dc field of 1300 Oe, the χ''_M *vs.* T plot still shows frequency-dependent tails of signals with maxima located close to the lowest accessible temperatures (Fig. 8), indicative of an efficient QTM relaxation process. This weak SMM behavior most likely results from the non-ideal coordination environments of the two crystallographically independent Dy^{III} atoms and the lack of any Ising-type molecular magnetic anisotropy for **2**.[34]

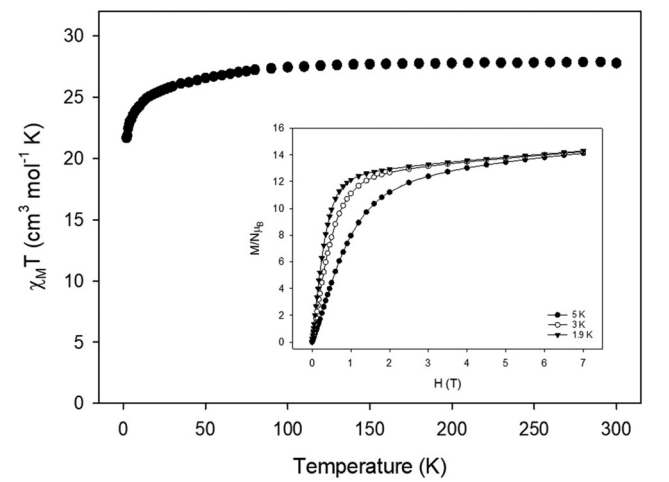

Fig. 7 Plot of $\chi_M T$ *vs.* T for complex $\{Dy_2\}$ (**2**) in a 0.1 T dc field. (Inset) Plot of magnetization (M) *vs.* field (H) for complex **2** at 1.9, 3 and 5 K in the range of 0–7 T dc field; the solid lines are guides for the eye only.

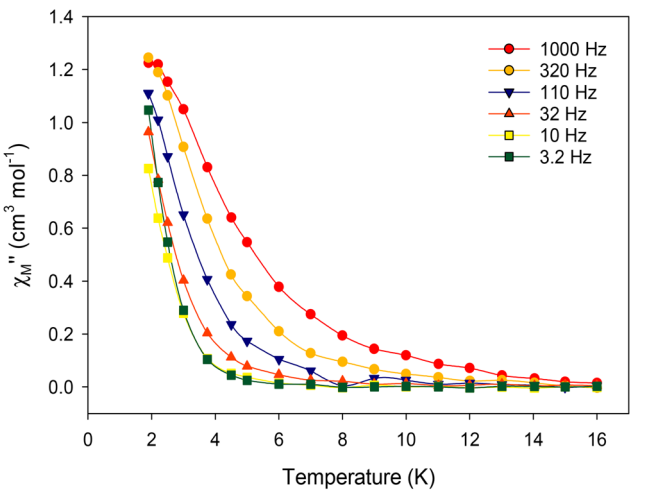

Fig. 8 Temperature dependence of the out-of-phase (χ''_M) ac magnetic susceptibility for complex $\{Dy_2\}$ (**2**) under an applied dc field of 1300 Oe measured in a 3.0 G ac field oscillating at the indicated frequencies; the solid lines are guides for the eye only.

The presence of a Mn^{III} ion linked to the $\{Ln_2\}$ subunits of the resulting heterometallic complexes **4** (Ln^{III} = Dy) and **5** (Ln^{III} = Gd), prompted us to investigate its effect on the magnetic properties of the $\{Mn^{III}Ln_2(\mu\text{-}O_2CR)_5\}^{4+}$ core. Direct-current (dc) magnetic susceptibility measurements were therefore performed on **4** and **5** in the 2–300 K range under an applied field of 0.1 T (Fig. 9, top). At 300 K, the $\chi_M T$ values of 33.83 cm^3 mol^{-1} K for **4** and 19.56 cm^3 mol^{-1} K for **5** are close to the theoretical values of 31.34 and 18.76 cm^3 mol^{-1} K, respectively, expected for one Mn^{III} (S = 2, g = 2) and two noninteracting Dy^{III} ions ($^6H_{15/2}$, S = 5/2, L = 5, g = 4/3) in **4**, or two Gd^{III} ions ($^8S_{7/2}$, S = 7/2, L = 0, g = 2) in **5**. Upon cooling, the $\chi_M T$ products of both compounds remain nearly constant till ~40 K and then increase rapidly, reaching the values of 38.39 cm^3 mol^{-1} K for **4** and 28.49 cm^3 mol^{-1} K for **5** at 2 K. This behaviour is indicative of dominant intramolecular ferromagnetic exchange interactions between the metal centers, clearly promoted by the presence of the Mn^{III} ion.

The field dependence of the magnetization for complexes **4** and **5** at 2, 3, and 5 K is shown in Fig. 9 (bottom). For the anisotropic complex **4**, a rapid increase in magnetization is observed at low fields, without reaching saturation up to ~7 T. This behavior indicates the presence of magnetic anisotropy arising from CF effects and/or depopulation of the M_J sublevels of the anisotropic Dy^{III} ions. At 7 T and 2 K, the magnetization reaches ~21.2$N\mu_B$, slightly lower than the theoretical value of 24.0$N\mu_B$ expected for one Mn^{III} and two Dy^{III} ions ($M_S/N\mu_B = n_{Mn}{\cdot}g_{Mn}{\cdot}S_{Mn} + n_{Dy}{\cdot}g_{Dy}{\cdot}J_{Dy}$). In contrast, complex **5** exhibits magnetization saturation above 5 T at 2 K, with a value of 18.0$N\mu_B$ at 7 T, in agreement with the expected value for one Mn^{III} and two Gd^{III} ions. This value corresponds to a ground state spin value of S_T = 9, consistent with a ferromagnetically coupled $\{Mn^{III}Gd_2\}$ system.

The magnetic susceptibility data for compound $\{Mn^{III}Gd_2\}$ (**5**) were fitted using PHI program,[35] to assess the nature and magnitude of the intramolecular $Mn^{III}\cdots Gd^{III}$ and $Gd^{III}\cdots Gd^{III}$ magnetic exchange interactions. On the basis of the triangular

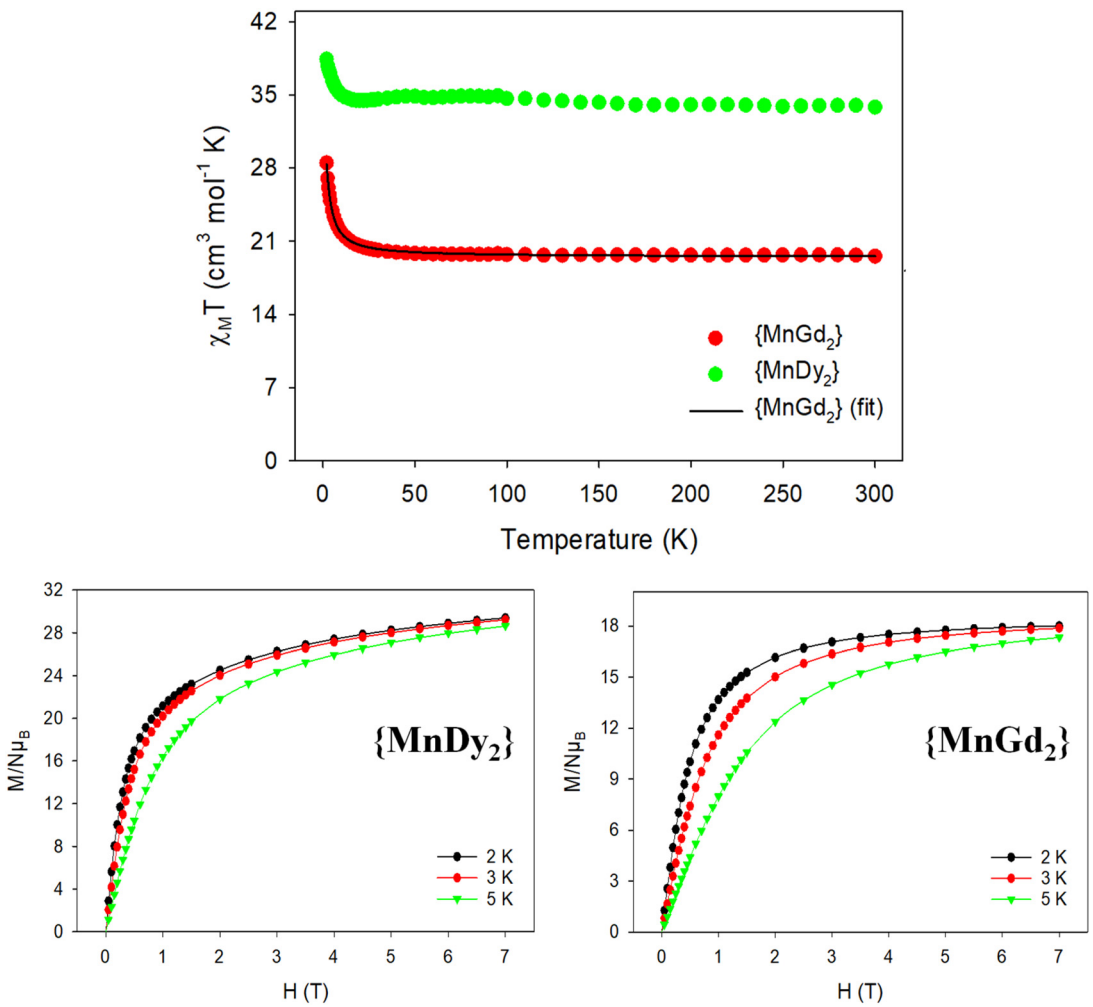

Fig. 9 (Top) Plots of $\chi_M T$ *vs.* T for complexes $\{Mn^{III}Dy_2\}$ (**4**) and $\{Mn^{III}Gd_2\}$ (**5**) in a 0.1 T dc field; the solid line in **5** is the best-fit curve (see the text for the fit parameters). (Bottom) Plots of magnetization (M) *vs.* field (H) for complexes $\{Mn^{III}Dy_2\}$ (**4**) and $\{Mn^{III}Gd_2\}$ (**5**) at 2, 3 and 5 K in range of 0–7 T dc field; the solid lines are guides for the eye only.

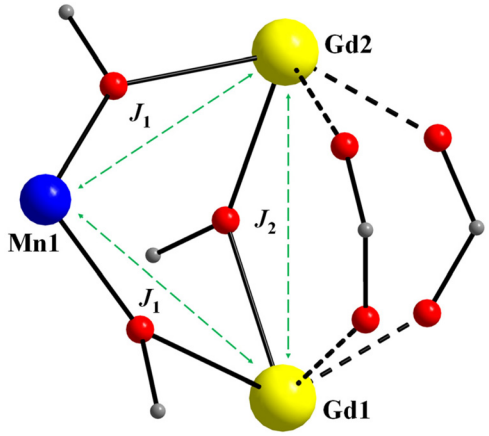

Fig. 10 *J*-Coupling scheme employed for the elucidation of the magnetic exchange interactions in complex $\{Mn^{III}Gd_2\}$ (**5**).

$\{Mn^{III}Gd_2\}$ core of **5**, the system was modelled using two exchange parameters: J_1 for the two equivalent $Mn^{III}\cdots Gd^{III}$ interactions and J_2 for the $Gd^{III}\cdots Gd^{III}$ interaction (Fig. 10). The corresponding spin Hamiltonian is given in eqn (1):

$$\hat{H} = -2J_1(\hat{S}_{Mn1}\hat{S}_{Gd1} + \hat{S}_{Mn1}\hat{S}_{Gd2}) - 2J_2(\hat{S}_{Gd1}\hat{S}_{Gd2}) \quad (1)$$

The best-fit parameters were $J_1 = +0.089(1)$ cm^{-1}, $J_2 = +0.005$ (1) cm^{-1} and $g = 2.04(2)$, indicating weak ferromagnetic $Mn^{III}\cdots Gd^{III}$ and $Gd^{III}\cdots Gd^{III}$ exchange interactions. The J_1 interaction between the Mn^{III} and Gd^{III} ions is mediated by a monoatomic RO^- bridge from the carboxylate moiety of a $sacb^{2-}$ ligand. In contrast, the much weaker J_2 interaction between the Gd^{III} ions originates from a monoatomic RO^- bridge from the carboxylate moiety of a $sacb^{2-}$ ligand combined with two *syn*,*syn*-carboxylate bridges provided by the $sacbH^-$ ligands. No intermolecular interaction term was required to obtain an excellent fit, supporting the intramolecular origin of the observed weak ferromagnetic exchange interactions and the resulting $S = 9$ spin ground state.

Unfortunately, no out-of-phase (χ''_M) signals were detected, either in the presence or absence of an external dc field, indicating the absence of SMM behavior for complexes **4** and **5**.

4. Concluding comments and perspectives

We have demonstrated that a metalloligand-assisted "LEGO®-brick" strategy can provide controlled access to structurally rare, low-nuclearity Mn^{III}/Ln^{III} clusters that are impossible (in our hands) to obtain through conventional one pot self-assembly reactions. The key synthetic element is the combination of the preformed mononuclear Mn^{III} complex $(Pr_2NH_2)[Mn^{III}(sacb)_2]$ (**1**), bearing available carboxylate donor atoms, with dinuclear lanthanide building blocks $[Ln_2(sacb)(sacbH)_3L(MeOH)]$ (Ln^{III} = Dy (**2**), Gd (**3**)). This stepwise approach afforded the heterometallic trinuclear complexes $[Mn^{III}Ln_2(sacb)_3(sacbH)_2L]$ (Ln^{III} = Dy (**4**), Gd (**5**)), which represent, to the best of our knowledge, the first examples of triangular $\{Mn^{III}Ln_2\}$ clusters and belong to the still very limited family of triangular $\{MLn_2\}$ compounds.

From a magnetic viewpoint, this work shows that incorporation of the Jahn–Teller active Mn^{III} ion has a pronounced effect on the magnetic behaviour of the lanthanide-based precursors. The Mn^{III}-free $\{Dy_2\}$ complex **2** exhibits a decrease of $\chi_M T$ at low temperature, mainly arising from crystal-field effects with a possible contribution from intramolecular antiferromagnetic $Dy^{III}\cdots Dy^{III}$ interactions, together with weak field-induced slow relaxation of magnetization. In contrast, the trinuclear $\{Mn^{III}Dy_2\}$ and $\{Mn^{III}Gd_2\}$ complexes display dominant ferromagnetic exchange interactions and an $S = 9$ ground state for the $\{Mn^{III}Gd_2\}$ analogue.

The absence of slow magnetic relaxation in **4** and **5** further emphasizes that high-spin ground states alone are not sufficient to produce SMM behaviour. In the Dy^{III}-containing trinuclear complex **4**, the magnetic dynamics are likely governed by the relative orientation of the local anisotropy axes and the efficiency of fast relaxation pathways. Future *ab initio* studies will therefore be important for clarifying the orientation of the Dy^{III} anisotropy axes, the composition of the ground and excited m_J states, and the role of the Jahn–Teller distorted Mn^{III} center in the relaxation process. More broadly, this work establishes preformed $\{Ln_2\}$ units as useful magnetic scaffolds that can be structurally modified through the rational incorporation of 3d-metal metalloligands, opening a route toward new families of predictable and magnetically informative 3d/4f clusters. Building on these findings, we are extending this "LEGO®-brick" approach to other trivalent 3d-metal ions, including diamagnetic Co^{III} and paramagnetic Cr^{III}/Fe^{III} centers, with the aim to accessing new families of predictable and magnetically interesting 3d/4f clusters.

Conflicts of interest

The authors declare no competing financial interest.

Data availability

The data supporting this article has been included as part of the supplementary information (SI). Supplementary information is available. See DOI: https://doi.org/10.1039/d6dt01428c.

CCDC 2559980, 2559981 and 2559982 (**2**, **4** and **5**, respectively) contain the supplementary crystallographic data for this paper.[36a–c]

Acknowledgements

This work has been supported by the funding program "MEDICUS" of the University of Patras (to D.I.A.). L.C.S. thanks the financial support received from the Fundação para a Ciência e Tecnologia and Ministério da Educação, Ciência e

Inovação (FCT/MECI) by PT national funds through the strategic project UID/50006/2025 (DOI 10.54499/UID/50006/2025) – Laboratório Associado para a Química Verde Tecnologias e Processos Limpos (LAQV/REQUIMTE).

References

1 (*a*) R. Sessoli, D. Gatteschi and J. Villain, in *Molecular Nanomagnets*, Oxford University Press, Oxford, UK, 2006; (*b*) C. Papatriantafyllopoulou, E. E. Moushi, G. Christou and A. J. Tasiopoulos, *Chem. Soc. Rev.*, 2016, **45**, 1597–1628.

2 (*a*) E. Moreno-Pineda and W. Wernsdorfer, *Adv. Quantum Technol.*, 2025, **8**, 2300367; (*b*) L. Bogani and W. Wernsdorfer, *Nat. Mater.*, 2008, **7**, 179–186; (*c*) D. Gatteschi and R. Sessoli, *Angew. Chem., Int. Ed.*, 2003, **42**, 268; (*d*) E. Coronado, *Nat. Rev. Mater.*, 2020, **5**, 87–104.

3 (*a*) R. Sessoli, H. Tsai, A. R. Schake, S. Wang, J. Vincent, K. Folting, D. Gatteschi, G. Christou and D. N. Hendrickson, *J. Am. Chem. Soc.*, 1993, **115**, 1804; (*b*) N. Mavragani and M. Murugesu, *Nat. Chem.*, 2025, **17**, 302; (*c*) C. J. Milios, A. Vinslava, W. Wernsdorfer, S. Moggach, S. Parsons, S. P. Perlepes, G. Christou and E. K. Brechin, *J. Am. Chem. Soc.*, 2007, **129**, 2754; (*d*) P. Abbasi, K. Quinn, D. I. Alexandropoulos, M. Damjanović, W. Wernsdorfer, A. Escuer, J. Mayans, M. Pilkington and Th. C. Stamatatos, *J. Am. Chem. Soc.*, 2017, **139**, 15644–15647.

4 (*a*) D. N. Woodruff, R. E. P. Winpenny and R. A. Layfield, *Chem. Rev.*, 2013, **113**, 5110–5148; (*b*) Z. Zhu, M. Guo, X.-L. Li and J. Tang, *Coord. Chem. Rev.*, 2019, **378**, 350–364; (*c*) J. Tang and P. Zhang, *Lanthanide Single Molecule Magnets*, Springer, 2015.

5 J.-L. Liu, Y.-C. Chen and M.-L. Tong, *Chem. Soc. Rev.*, 2018, **47**, 2431–2453.

6 Representative examples: (*a*) A. Dey, P. Kalita and V. Chandrasekhar, *ACS Omega*, 2018, **3**, 9462–9475; (*b*) J. Liu, Y.-C. Chen, J.-L. Liu, V. Vieru, L. Ungur, J.-H. Jia, L. F. Chibotaru, Y. Lan, W. Wernsdorfer, S. Gao, X.-M. Chen and M.-L. Tong, *J. Am. Chem. Soc.*, 2016, **138**, 5441–5450; (*c*) W. Xu, Q. Luo, Z. Li, Y. Zhai and Y. Zheng, *Adv. Sci.*, 2024, **11**, 2308548; (*d*) A. S. Armenis, A. Mondal, S. R. Giblin, D. I. Alexandropoulos, J. Tang, R. A. Layfield and Th. C. Stamatatos, *Inorg. Chem. Front.*, 2025, **12**, 1214–1224; (*e*) F. S. Guo, B. M. Day, Y. C. Chen, M. L. Tong, A. Mansikkamäki and R. A. Layfield, *Science*, 2018, **362**, 1400–1403.

7 N. Ishikawa, M. Sugita, T. Ishikawa, S. Koshihara and Y. Kaizu, *J. Am. Chem. Soc.*, 2003, **125**, 8694.

8 Representative examples: (*a*) F. Habib and M. Murugesu, *Chem. Soc. Rev.*, 2013, **42**, 3278; (*b*) J. Tian, J. Du, B. Li, H. Zhang, Y. Zhang, L. Sun and P. Ma, *J. Mater. Chem. C*, 2024, **12**, 14754–14773; (*c*) P. Lin, T. J. Burchell, R. Clérac and M. Murugesu, *Angew. Chem., Int. Ed.*, 2008, **47**, 8848–8851; (*d*) Y.-N. Guo, G.-F. Xu, W. Wernsdorfer, L. Ungur, Y. Guo, J. Tang, H.-J. Zhang, L. F. Chibotaru and A. K. Powell, *J. Am. Chem. Soc.*, 2011, **133**, 11948–11951; (*e*) J. Long, F. Habib, P.-H. Lin, I. Korobkov, G. Enright, L. Ungur, W. Wernsdorfer, L. F. Chibotaru and M. Murugesu, *J. Am. Chem. Soc.*, 2011, **133**, 5319–5328; (*f*) F. Habib, G. Brunet, V. Vieru, I. Korobkov, L. F. Chibotaru and M. Murugesu, *J. Am. Chem. Soc.*, 2013, **135**, 13242–13245.

9 S. Osa, T. Kido, N. Matsumoto, N. Re, A. Pochaba and J. Mrozinski, *J. Am. Chem. Soc.*, 2004, **126**, 420–421.

10 L. R. Piquer and E. C. Sañudo, *Dalton Trans.*, 2015, **44**, 8771–8780.

11 (*a*) M. Holynska, D. Premuzic, I.-R. Jeon, W. Wernsdorfer, R. Clérac and S. Dehnen, *Chem. – Eur. J.*, 2011, **17**, 9605–9610; (*b*) V. Mereacre, A. M. Ako, R. Clerac, W. Wernsdorfer, I. J. Hewitt, C. E. Anson and A. K. Powell, *Chem. – Eur. J.*, 2008, **14**, 3577; (*c*) M. Zaleski, E. C. Depperman, J. W. Kampf, M. L. Kirk and V. L. Pecoraro, *Angew. Chem., Int. Ed.*, 2004, **43**, 3912; (*d*) V. Mereacre, A. M. Ako, R. Clerac, W. Wernsdorfer, G. Filoti, J. Bartolome, C. E. Anson and A. K. Powell, *J. Am. Chem. Soc.*, 2007, **129**, 9248; (*e*) Th. C. Stamatatos, S. J. Teat, W. Wernsdorfer and G. Christou, *Angew. Chem., Int. Ed.*, 2009, **48**, 521; (*f*) A. Mishra, W. Wernsdorfer, K. A. Abboud and G. Christou, *J. Am. Chem. Soc.*, 2004, **126**, 15648; (*g*) J. L. Liu, F. S. Guo, Z. S. Meng, Y. Z. Zheng, J. D. Leng, M. L. Tong, L. Ungur, L. F. Chibotaru, K. J. Heroux and D. N. Hendrickson, *Chem. Sci.*, 2011, **2**, 1268; (*h*) A. M. Ako, V. Mereacre, R. Clerac, W. Wernsdorfer, I. J. Hewitt, C. E. Anson and A. K. Powell, *Chem. Commun.*, 2009, 544; (*i*) C. Papatriantafyllopoulou, W. Wernsdorfer, K. A. Abboud and G. Christou, *Inorg. Chem.*, 2011, **50**, 421.

12 Representative examples: (*a*) J. Tang, I. Hewitt, N. T. Madhu, G. Chastanet, W. Wernsdorfer, C. E. Anson, C. Benelli, R. Sessoli and A. K. Powell, *Angew. Chem., Int. Ed.*, 2006, **45**, 1729–1733; (*b*) C. Lampropoulos, K. A. Abboud, Th. C. Stamatatos and G. Christou, *Inorg. Chem.*, 2009, **48**, 813–815; (*c*) Y.-X. Wang, W. Shi, H. Li, Y. Song, L. Fang, Y. Lan, A. K. Powell, W. Wernsdorfer, L. Ungur, L. F. Chibotaru, M. Shen and P. Cheng, *Chem. Sci.*, 2012, **3**, 3366; (*d*) C. G. Efthymiou, C. P. Raptopoulou, V. Psycharis, A. J. Tasiopoulos, A. Escuer, S. P. Perlepes and C. Papatriantafyllopoulou, *Polyhedron*, 2013, **64**, 30–37; (*e*) T. Pugh, F. Tuna, L. Ungur, D. Collison, E. J. L. McInnes, L. F. Chibotaru and R. A. Layfield, *Nat. Commun.*, 2015, **6**, 7492; (*f*) Th. C. Stamatatos, D. Foguet-Albiol, C. C. Stoumpos, C. P. Raptopoulou, A. Terzis, W. Wernsdorfer, S. P. Perlepes and G. Christou, *J. Am. Chem. Soc.*, 2005, **127**, 15380–15381; (*g*) B. S. Dolinar, D. I. Alexandropoulos, K. R. Vignesh, T. James and K. R. Dunbar, *J. Am. Chem. Soc.*, 2018, **140**, 908–911; (*h*) S.-Y. Lin, Y.-N. Guo, Y. Guo, L. Zhao, P. Zhang, H. Ke and J. Tang, *Chem. Commun.*, 2012, **48**, 6924; (*i*) T. Sato, F. Ambe, K. Endo, M. Katada, H. Maeda, T. Nakamoto and H. Sano, *J. Am. Chem. Soc.*, 1996, **118**, 3450–3458; (*j*) C. Wilson, B. B. Iversen, J. Overgaard, F. K. Larsen, G. Wu, S. P. Palii, G. A. Timco and N. V. Gerbeleu, *J. Am.*

Chem. Soc., 2000, **122**, 11370–11379; (*k*) Th. C. Stamatatos, D. Foguet-Albiol, S.-C. Lee, C. C. Stoumpos, C. P. Raptopoulou, A. Terzis, W. Wernsdorfer, S. O. Hill, S. P. Perlepes and G. Christou, *J. Am. Chem. Soc.*, 2007, **129**, 9484–9499; (*l*) A. Figuerola, V. Tangoulis, J. Ribas, H. Hartl, I. Brüdgam, M. Maestro and C. Diaz, *Inorg. Chem.*, 2007, **46**, 11017–11024; (*m*) C. G. Efthymiou, C. P. Raptopoulou, A. Terzis, S. P. Perlepes, A. Escuer and C. Papatriantafyllopoulou, *Polyhedron*, 2010, **29**, 627–633.

13 Representative examples: (*a*) R. Bag, Y. Sikdar, P. Saha, P. Ghosh, M. G. B. Drew, J. Tang and S. Goswami, *New J. Chem.*, 2021, **45**, 5258–5265; (*b*) P.-E. Car, A. Favre, A. Caneschi and R. Sessoli, *Dalton Trans.*, 2015, **44**, 15769–15773; (*c*) A. Bencini, C. Benelli, A. Caneschi, R. L. Carlin, A. Dei and D. Gatteschi, *J. Am. Chem. Soc.*, 1985, **107**, 8128–8136; (*d*) S. Xue, L. Ungur, Y.-N. Guo, J. Tang and L. F. Chibotaru, *Inorg. Chem.*, 2014, **53**, 12658–12663; (*e*) M. Savva, D. I. Alexandropoulos, M. Pissas, S. P. Perlepes, C. Papatriantafyllopoulou, Y. Sanakis and A. J. Tasiopoulos, *Dalton Trans.*, 2023, **52**, 6997–7008; (*f*) C. G. Efthymiou, A. N. Georgopoulou, C. Papatriantafyllopoulou, A. Terzis, C. P. Raptopoulou, A. Escuer and S. P. Perlepes, *Dalton Trans.*, 2010, **39**, 8603; (*g*) A. S. Armenis, V. Vipanchi, K. N. Pantelis, L. Cunha-Silva, K. R. Vignesh, D. I. Alexandropoulos and Th. C. Stamatatos, *Chem. – Eur. J.*, 2023, **29**, e202302337; (*h*) N. Singh, S. Das Gupta, R. J. Butcher and G. Christou, *Dalton Trans.*, 2017, **46**, 7897–7903; (*i*) S. Mukherjee, M. R. Daniels, R. Bagai, K. A. Abboud, G. Christou and C. Lampropoulos, *Polyhedron*, 2010, **29**, 54–65.

14 G. Christou, *Polyhedron*, 2005, **24**, 2065–2075.

15 (*a*) G. Kumar and R. Gupta, *Chem. Soc. Rev.*, 2013, **42**, 9403; (*b*) C. Papatriantafyllopoulou, M. Estrader, C. G. Efthymiou, D. Dermitzaki, K. Gkotsis, A. Terzis, C. Diaz and S. P. Perlepes, *Polyhedron*, 2009, **28**, 1652–1655; (*c*) K. N. Pantelis, C. P. Raptopoulou, V. Psycharis, J. Tang and Th. C. Stamatatos, *Dalton Trans.*, 2025, **54**, 977–988.

16 (*a*) K. N. Pantelis, G. Karotsis, C. Lampropoulos, L. Cunha-Silva, A. Escuer and Th. C. Stamatatos, *Materials*, 2020, **13**, 1352; (*b*) E. C. Mazarakioti, J. Regier, L. Cunha-Silva, W. Wernsdorfer, M. Pilkington, J. Tang and Th. C. Stamatatos, *Inorg. Chem.*, 2017, **56**, 3568–3578; (*c*) A. A. Athanasopoulou, M. Pilkington, C. P. Raptopoulou, A. Escuer and Th. C. Stamatatos, *Chem. Commun.*, 2014, **50**, 14942–14945; (*d*) P. S. Perlepe, A. A. Athanasopoulou, K. I. Alexopoulou, C. P. Raptopoulou, V. Psycharis, A. Escuer, S. P. Perlepes and Th. C. Stamatatos, *Dalton Trans.*, 2014, **43**, 16605–16609; (*e*) A. A. Athanasopoulou, C. P. Raptopoulou, A. Escuer and Th. C. Stamatatos, *RSC Adv.*, 2014, **4**, 12680–12684; (*f*) K. N. Pantelis, K. H. Baka, L. Cunha-Silva, J. Tang, D. I. Alexandropoulos and Th. C. Stamatatos, *Cryst. Growth Des.*, 2025, **25**, 4553–4564; (*g*) K. N. Pantelis, D. I. Alexandropoulos, A. Escuer, G. E. Kostakis and T. C. Stamatatos, *CrystEngComm*, 2026, **28**, 112–122.

17 G. A. Bain and J. F. Berry, *J. Chem. Educ.*, 2008, **85**, 532.

18 T. Kottke and D. Stalke, *J. Appl. Crystallogr.*, 1993, **26**, 615–619.

19 *APEX2, Data Collection Software Version 2012.4*, Bruker AXS, Delft, The Netherlands, 2012.

20 *Cryopad, Remote Monitoring and Control, Version 1.451*, Oxford Cryosystems, Oxford, UK, 2006.

21 *SAINT+, Data Integration Engine v. 7.23a ©*, Bruker AXS, Madison, WI, USA, 1997–2005.

22 G. M. Sheldrick, *SADABS v.2.01. Bruker/Siemens Area Detector Absorption Correction Program*, Bruker AXS, Madison, WI, USA, 1998.

23 L. Palatinus and G. Chapuis, *J. Appl. Crystallogr.*, 2007, **40**, 786–790.

24 (*a*) G. M. Sheldrick, *Acta Crystallogr., Sect. C: Struct. Chem.*, 2015, **71**, 3–8; (*b*) O. V. Dolomanov, L. J. Bourhis, R. J. Gildea, J. A. K. Howard and H. Puschmann, *J. Appl. Crystallogr.*, 2009, **42**, 339–341.

25 (*a*) A. L. Spek, *J. Appl. Crystallogr.*, 2003, **36**, 7–13; (*b*) A. L. Spek, *Acta Crystallogr., Sect. D: Biol. Crystallogr.*, 2009, **65**, 148–155; (*c*) A. L. Spek, *Acta Crystallogr., Sect. C: Struct. Chem.*, 2015, **71**, 9–18.

26 K. Brandenburg, *DIAMOND, Release 3. 1f*, Crystal Impact GbR, Bonn, Germany, 2008, p. 389.

27 I. J. Bruno, J. C. Cole, P. R. Edgington, M. K. Kessler, C. F. Macrae, P. McCabe, J. Pearson and R. Taylor, MERCURY, *Acta Crystallogr., Sect. B: Struct. Sci.*, 2002, **58**, 389.

28 K. Nakamoto, *Infrared and Raman Spectra of Inorganic and Coordination Compounds*, Wiley, New York, USA, 4th edn, 1986.

29 W. Liu and H. H. Thorp, *Inorg. Chem.*, 1993, **32**, 4102.

30 M. Llunell, D. Casanova, J. Girera, P. Alemany and S. Alvarez, *SHAPE; Version 2.0*, Universitat de Barcelona, Barcelona, Spain, 2010.

31 Representative examples: (*a*) L. Liang, G. Peng, G. Li, Y. Lan, A. K. Powell and H. Deng, *Dalton Trans.*, 2012, **41**, 5816–5823; (*b*) W. Wang, H. Zhang, S. Wang, H. Shen, H. Gao, J. Cui and B. Zhao, *Inorg. Chem.*, 2015, **54**, 10610–10622; (*c*) L. Zhang, J. Jung, P. Zhang, M. Guo, L. Zhao, J. Tang and B. Le Guennic, *Chem. – Eur. J.*, 2016, **22**, 1392–1398; (*d*) J. Zhang, H. Zhang, Y. Chen, X. Zhang, Y. Li, W. Liu and Y. Dong, *Dalton Trans.*, 2016, **45**, 16463–16470; (*e*) A. S. Armenis, A. Worrell, D. I. Alexandropoulos, J. Tang and Th. C. Stamatatos, *Cryst. Growth Des.*, 2024, **24**, 9243–9253.

32 (*a*) X.-L. Li, F.-Y. Min, C. Wang, S.-Y. Lin, Z. Liu and J. Tang, *Dalton Trans.*, 2015, **44**, 3430–3438; (*b*) N. F. Ghazali, K. R. Vignesh, W. Phonsri, K. S. Murray, P. C. Junk, G. B. Deacon and D. R. Turner, *Dalton Trans.*, 2022, **51**, 18502–18513; (*c*) C. Chen, J.-J. Yin, J. Zheng and X.-Y. Zheng, *Polyhedron*, 2020, **190**, 114757; (*d*) C. Lampropoulos, Th. C. Stamatatos, K. A. Abboud and G. Christou, *Inorg. Chem.*, 2009, **48**, 429–431.

33 Representative examples: (*a*) H. Ke, S. Zhang, X. Li, Q. Wei, G. Xie, W. Wang and S. Chen, *Dalton Trans.*, 2015, **44**, 21025–21031; (*b*) M. Dolai, E. Moreno-Pineda,

W. Wernsdorfer, M. Ali and A. Ghosh, *J. Phys. Chem. A*, 2021, **125**, 8230–8237; (*c*) P. Bag, C. K. Rastogi, S. Biswas, S. Sivakumar, V. Mereacre and V. Chandrasekhar, *Dalton Trans.*, 2015, **44**, 4328–4340; (*d*) S. Lin, J. Wu, C. Wang, L. Zhao and J. Tang, *Eur. J. Inorg. Chem.*, 2015, **2015**, 5488–5494; (*e*) D.-D. Feng, F. Lu, Z.-Y. Liu, X.-G. Wang, X.-C. Li, E.-C. Yang, Y.-Q. Zhang and X.-J. Zhao, *Inorg. Chem.*, 2022, **61**, 13133–13142; (*f*) H.-J. Ye, T. Zhang, S.-Y. Huang, X.-L. Liu, W.-B. Chen, Y.-Q. Zhang, J. Tang and W. Dong, *Dalton Trans.*, 2021, **50**, 13728–13736; (*g*) S. Xue, Y.-N. Guo, L. Ungur, J. Tang and L. F. Chibotaru, *Chem. – Eur. J.*, 2015, **21**, 14099–14106.

34 A. S. Armenis, G. P. Bakali, C. L. Brantley, C. P. Raptopoulou, V. Psycharis, L. Cunha-Silva, G. Christou and Th. C. Stamatatos, *Dalton Trans.*, 2022, **51**, 18077–18089.

35 N. F. Chilton, R. P. Anderson, L. D. Turner, A. Soncini and K. S. Murray, *J. Comput. Chem.*, 2013, **34**, 1164.

36 (*a*) CCDC 2559980: Experimental Crystal Structure Determination, 2026, DOI: 10.5517/ccdc.csd.cc2rxw0l; (*b*) CCDC 2559981: Experimental Crystal Structure Determination, 2026, DOI: 10.5517/ccdc.csd.cc2rxw1m; (*c*) CCDC 2559982: Experimental Crystal Structure Determination, 2026, DOI: 10.5517/ccdc.csd.cc2rxw2n.